Hindawi
Mathematical Problems in Engineering
Volume 2022, Article ID 5289401, 18 pages
https://doi.org/10.1155/2022/5289401

Research Article

Flow Analysis of Two-Layer Nano/Johnson–Segalman Fluid in a Blood Vessel-like Tube with Complex Peristaltic Wave

A. Zeeshan,[1] **A. Riaz**,[2] **Faris Alzahrani**,[3] **and A. Moqeet**[1]

[1]*Department of Mathematics & Statistics, FBAS, International Islamic University Islamabad, H-10, Islamabad, Pakistan*
[2]*Department of Mathematics, Division of Science and Technology, University of Education, Lahore 54770, Pakistan*
[3]*Department of Mathematics, Faculty of Sciences, King Abdulaziz University, P. O. Box 80203, Jeddah 21589, Saudi Arabia*

Correspondence should be addressed to A. Zeeshan; ahmad.zeeshan@iiu.edu.pk

Received 17 November 2021; Revised 6 January 2022; Accepted 15 January 2022; Published 25 February 2022

Academic Editor: Ali Ahmadian

Biologically inspired micropumps using the phenomena of peristalsis are highly involved in targeted drugging in pharmacological engineering. This study analyzed theoretically the transport of two immiscible fluids in a long flexible tube. The core region contains Johnson–Segalman non-Newtonian fluid, while the peripheral region is saturated by nanofluid. It is assumed that Darcy's porous medium is encountered close to the walls of the tube. A complex peristaltic wave is transmitted on the compliant wall which induces the flow. Equations of continuity, momentum, energy, and nanoparticle concentration are used in modelling the problem. The modelled problem for both the regions, i.e., core and peripheral regions are developed with the assumptions of long wavelength and creeping flow. Temperature, velocity, and shear stress at the interface are assumed to be equal. The system of equations is solved analytically. The graphical results for different involving parameters are displayed and thoroughly discussed. It is received that the heat transfer goes inverse with fluid viscosity in the peripheral region, but opposite measurements are obtained in the core region. This theoretical model may be considerable in some medical mechanisms such as targeted drug delivery, differential diagnosis, and hyperthermia. Moreover, no study on non-Newtonian nanofluid is reported yet for the two-layered flow system, so this study will give a good addition in the literature of biomedical research.

1. Introduction

The transport of fluid in a channel or tube due to contraction and relaxation of flexible walls are known as peristalsis. It can be observed naturally in the human body for the transport of food, some blood vessels, movement of spermatozoa and ovum in reproductive track, and many other body systems. Phenomena inspired scientists and leads to many biomedical instruments and other transport techniques in machines such as a heart-lung machine and PDMS peristaltic micropump [1, 2]. Other than biomedical devices, it can be employed in devices such as sanitary transport.

Latham [3] experimentally elaborated the phenomena, leading to numerous investigations [4–8] allocated in the domain of peristaltic flow for different flow geometries and under various assumptions. Jaffrin and Shapiro [9] initiated the study of peristaltic transport with low Reynold's number approximation. Most recently, Zeeshan et al. [10] investigated the rheological features of nanofluid in a rectangular duct driven by a complex peristaltic wave. The effect of electrophoresis was focused and the analytic solution is found. They revealed that the change in amplitude ratios of complex waves affects the flow positively, that is, more bolus are observed. Tripathi et al. [11] theoretically studied the transport phenomena of a nanofluid due to complex peristaltic transportation with effects of electro-osmosis. The analysis focuses on nanofluids, and they observe the effects of the rise in Joule's heating, thermophoresis, Brownian motion, Grashoff number, etc. Javid et al. [12] described the peristaltic propulsion of viscous fluid in a channel with a complex wave. They used numerical simulations to evaluate the results. The evaluation further focused on magnetohydrodynamics which enhances the worth of study. Furthermore, Tripathi et al. [13] added electrodynamical effects with

a couple stress fluids in ocular flow. Bhatti et al. [14] argued two-phase flow in a channel with a compliant wall.

Usually, in biological systems, such as the ureter, oesophagus, or small veins, it became apparent that the walls are lubricated with a film of fluid. These fluids may be different in nature rheologically and continuously pumped out. Recently, some researchers [15, 16] have shown experimentally that the blood flux in tiny veins has an outer stratum made of plasma (which is usually Newtonian fluid), whereas an inner stratum called core possesses red blood (usually modelled as non-Newtonian fluid). The fluid rheologies may vary in different transport ducts of the human body. The study motivated some recent literature in physiological flow two-layer immiscible fluids' flow analysis.

Maybe, the first mathematical analysis in this domain was performed by Srivastava and Srivastava [17] back in 1982. They considered both Newtonian fluids with different viscosities and compared the results with experimental results of Weinberg et al. [18].

Misra and Pandey [19] then use the model for the transport of blood in small blood vessels. They use the Casson model for core region flow and Newtonian fluid close to the wall. They concluded the denser the peripheral fluid is, the higher the flow rate of the core region is.

More recently, Vajravelu and Saravana [20] examined the two-layered fluid model with non-Newtonian Jeffery fluid in the core region, and Newtonian fluid is taken close to walls in a channel with heat transfer and fluid slip effects. Ali et al. [21] worked on peristaltic transport in an axisymmetric tube with FENE-P fluid in the core region. They focused on electro-osmosis effects. Again, Ali et al. [22] reported similar flow with Ellis fluid in the core region. Rajashekhar et al. [23] assumed the Herschel–Bulkley model for the flow in the core region of so-called blood flow. Tripathi et al. [11] worked on Bingham and power-law fluid in a channel. The results are extended for three-layer fluids by Tripathi et al. [24] and were reported in 2017.

Mathematical simulations of many biologically inspired systems are developed and produced effect outputs in finding the cure or histories of many biologically inspired systems. Since decades, these models and simulation are vital in reducing animal experimentation [25–29]. So, major contributions of the current work can be overviewed as

(i) This article endures some novel applications of the flow of two-layer fluid in a flexible tube.

(ii) The complex peristaltic wave travels along the surface of the tube. As described by Dobrolyubov and Douchy [30] that the geometric form of a peristaltic wave in the intestine is complex most of the time, therefore, this study is an effort to describe flow as close to the real physiological problem as possible.

(iii) The two-layer flow of nanofluid and Johnson–Segalman fluid in the flexible tube with a compliant wall is evaluated analytically along with the effects of the partial porous medium and catheter.

The creeping flow and long-wavelength approximation are assumed and perturbation is employed to evaluate the solution. Structure of the investigation is arranged as follows. Section 2 discusses the mathematical modelling of the whole phenomenon through geometrical description and derivations of the quantitative expressions from main physical laws. Section 3 suggests the methodology of the solution to handle the obtained systems of equations. In Section 4, results are revealed in the form of graphs and tables and discussed with profound depth. Lastly, a few significant conclusions are drawn from the recent investigation and are furnished in Section 5.

2. Theory and Mathematical Model

2.1. Geometry of the Problem. An infinitely long circular axisymmetric co-centric cylinder, as illustrated in Figure 1, is the area of interest in current communication. Furthermore, a complex sinusoidal wave travels along z-axis on the outer cylinder which is passing through the centre of pipe along with wavelength λ, speed of wave c, amplitudes b_i, and the pipe radius a_0. The inner pipe has a radius of a_ϵ and is considered stationary. The motion of wave on a flexible wall is mathematically defined as

$$R_0(z,t) = \pm a_0 \pm b_1 \cos\left[\frac{2\pi}{\lambda}(z-ct)\right] \pm b_2 \cos\left[\frac{4\pi}{\lambda}(z-ct)\right]. \tag{1}$$

Mathematically inner cylinder can be represented as

$$R_\epsilon(z,t) = a_\epsilon. \tag{2}$$

Here, z designates the direction of propagation of the wave, i.e., parallel to the z-axis. The outer cylinder is kept at a temperature T_1, while the inner cylinder is at a temperature $T_0 < T_1$ The core region is also assumed to be saturated by non-Newtonian Johnson–Segalman fluid. While region close to the outer pipe wall is porous and is saturated by Newtonian nanofluid. Both the fluids are immiscible and separated at

$$R(z,t) = a_1. \tag{3}$$

2.2. Porous Media. A porous medium is a space defined by solid with void space uniformly distributed in the whole region, which allows fluid to transport but with some resistive force called Darcy's forces. These mediums help to uphold the heat in porous systems. The application and usage of porous media in engineering can be underlined in various fields such as petroleum engineering, rock and soil mechanics, hydrogeology, and, more recently, in bioengineering and biology. Many scientists have established their interest in considering heat transfer biologically inspired flow in permeable domains [31–35].

The basic feature of the porous medium is porosity which can be defined as the ratio of the volume of free space

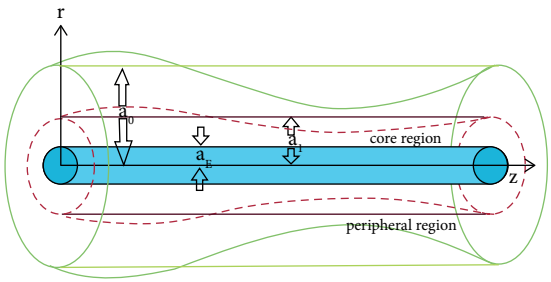

Figure 1: Geometry of the problem.

to the volume of the full body. Usually, the value of porosity is 0.45, with dense materials and compact structure; it reduces to 0.25 and so.

The velocity V of fluid flow hinges on permeability and pressure gradient as defined by the modified Darcy equation:

$$-\frac{dp}{dy} = \alpha\mu V + \beta\rho V^2. \tag{4}$$

Here, the coefficient α defines loss due to friction generated by the viscosity of fluid and shape of a porous medium. The inertial parameter β incorporates loss in inertial due to bend in porous spaces and other factors; it is proportional to ρV2.

The modified Darcy equation is universal relation and defines fluid flow in porous spaces.

At a low Reynolds number, the inertial term in equation (1) can be neglected and becomes

$$-\frac{dp}{dy} = \frac{\mu}{K}V. \tag{5}$$

Here, $K = 1/\alpha$ is known as the Darcy permeability.

2.3. Nanofluids. A solid-liquid suspension is engineered in such a way that nanosized particles are uniformly distributed and do not agglomerate in a base fluid. These nanosized particles are usually oxides and carbides of metal or carbon nanotubes. Base fluid can be any liquid that is oils or water with low thermal conductivity. These fluids exhibit enhanced thermal conductivity which makes it imperative to gain knowledge of the rheology of nanofluid before its usage. Application of these fluids is in solar energy storage, microelectronics, fuel cells, pharmaceutical process, hybrid engines, chillers, and other machines related to heat transfer. Nanofluids also show special properties with the magnetic field, acoustics and ultrasound, etc. [36–40].

Mathematical models of this fluid was described by Buongiorno [41]. He observed an abnormal increase in thermal conductivity, viscosity, and heat transfer rate coefficient. It is due to the nanofluid property of the thermophoresis and Brownian motion.

If J is diffusion mass flux of the nanoparticle w.r.t. fluid velocity, then it can be written as the sum of Brownian motion and thermophoresis; if no external force is applied,

$$-\frac{1}{\rho}\nabla\cdot\mathbf{J} = \frac{\partial\varphi}{\partial t} + \mathbf{V}\cdot\nabla\varphi = \nabla\cdot\left[\mathbf{D_B}\nabla\varphi + \mathbf{D_B}\frac{\nabla T}{T}\right], \tag{6}$$

where φ is the concentration of nanoparticles and D_B and DT are due to the slip velocity of particles caused by Brownian motion and thermophoresis. The energy equations for nanofluids are

$$\rho c\left[\frac{\partial\mathbf{T}}{\partial t} + \mathbf{V}\cdot\nabla\mathbf{T}\right] = -\nabla\cdot\mathbf{q} + h_p\nabla\cdot\mathbf{J}. \tag{7}$$

Neglecting radiative heat transfer, q can be calculated as the conduction heat flux, c is heat capacity, and h_p is specific enthalpy.

2.4. Constitutive Equation of Johnson–Segalman Fluid. The Johnson–Segalman fluid [42] defines nonmonotonically related shear stress and rate of shear for some values of the parameter of material. Spurt is an example of the property of this model.

Johnson and Segalman initially suggested an integral approach to the model, but rate type form can be derived. Considering appropriate parameters, the mathematical form of Johnson Segalman fluid [43] can be written as

$$\begin{aligned} S + \lambda\left(\frac{DS}{Dt} + S(W - a\ D) + (W - a\ D)^T S\right) &= 2\mu\ D, \\ T &= -2\mu\ D + S, \\ \sigma &= -pI + T. \end{aligned} \tag{8}$$

Here, $W = 1/2[L - L^T]$ is skew-symmetric and $D = 1/2[L - L^T]$ is symmetric part of velocity gradient, D/Dt is material derivative, λ is relaxation time, and a is called slip coefficient. The special case of this model can be achieved if

(a) $a = 1$: it becomes Olyroyd-B model

(b) $a = 1$ and $\mu = 0$: Maxwell model

(c) $\lambda = 0$: Newtonian fluid

2.5. Flow Problem. Modelling of flow in fluid transport problems usually involves four equations each, i.e.,

(i) Continuity equation as a consequence of the law of conservation of mass

(ii) Momentum equation due to law of conservation of momentum

(iii) Energy equation as defined by the law of conservation of energy

(iv) Nanoparticle concentration equation

In current communication, these equations are divided into two regions so-called core and the peripheral region.

The core region is saturated with Johnson–Segalman fluid and the porous peripheral region is filled with a nanofluid.

2.5.1. Peripheral Region

$$\left(\frac{\partial C}{\partial t}+\overline{u}\frac{\partial C}{\partial \overline{z}}+w\frac{\partial C}{\partial r}\right)=D_b\left(\frac{\partial^2 C}{\partial \overline{z}^2}+\frac{\partial^2 C}{\partial \overline{r}^2}+\frac{1}{\overline{r}}\frac{\partial C}{\partial \overline{r}}\right)+\frac{D_t}{T_0}\left(\frac{\partial^2 T}{\partial \overline{z}^2}+\frac{\partial^2 T}{\partial \overline{r}^2}+\frac{1}{\overline{r}}\frac{\partial T}{\partial \overline{r}}\right),$$

$$\rho c_p\left(\frac{\partial T}{\partial t}+\overline{u}\frac{\partial T}{\partial \overline{z}}+w\frac{\partial \overline{v}}{\partial r}\right)=k\left(\frac{\partial^2 T}{\partial \overline{z}^2}+\frac{\partial^2 T}{\partial \overline{r}^2}+\frac{1}{\overline{r}}\frac{\partial T}{\partial \overline{r}}\right),$$

$$+\mu\left(2\left(\left(\frac{\partial u}{\partial \overline{r}}\right)^2+\left(\frac{\partial w}{\partial \overline{z}}\right)^2\right)+\left(\frac{\partial u}{\partial z}+\frac{\partial w}{\partial r}\right)^2\right),$$

$$+\tau\begin{pmatrix} D_b\left(\dfrac{\partial C}{\partial \overline{r}}\dfrac{\partial T}{\partial \overline{r}}+\dfrac{\partial C}{\partial \overline{z}}\dfrac{\partial T}{\partial \overline{z}}\right)+ \\ \dfrac{D_t}{T}\left(\left(\dfrac{\partial T}{\partial \overline{r}}\right)^2+\left(\dfrac{\partial T}{\partial \overline{z}}\right)^2\right)\end{pmatrix}, \tag{9}$$

$$-\frac{\mu}{K}w+\rho g\beta\left(T-T_0\right)+\rho g\beta\left(C-C_0\right),$$

$$\rho\left(\frac{\partial w}{\partial t}+\overline{u}\frac{\partial w}{\partial \overline{z}}+w\frac{\partial w}{\partial r}\right)=-\frac{\partial \overline{p}}{\partial z}+\mu\left(\frac{\partial^2 w}{\partial \overline{z}^2}+\frac{\partial^2 w}{\partial \overline{r}^2}+\frac{1}{\overline{r}}\frac{\partial w}{\partial \overline{r}}\right),$$

$$\rho\left(\frac{\partial \overline{u}}{\partial t}+\overline{u}\frac{\partial \overline{u}}{\partial \overline{z}}+w\frac{\partial \overline{u}}{\partial r}\right)=-\frac{\partial \overline{p}}{\partial r}+\mu\left(\frac{\partial^2 \overline{u}}{\partial \overline{z}^2}+\frac{\partial^2 \overline{u}}{\partial \overline{r}^2}+\frac{1}{\overline{r}}\frac{\partial \overline{u}}{\partial \overline{r}}\right),$$

$$\frac{\partial \overline{u}}{\partial \overline{z}}+\frac{1}{\overline{r}}\frac{\partial\left(w\overline{r}\right)}{\partial \overline{r}}=0.$$

2.5.2. Core Region

$$\frac{\partial \overline{u}}{\partial \overline{z}}+\frac{1}{\overline{r}}\frac{\partial\left(w\overline{r}\right)}{\partial \overline{r}}=0, \tag{10}$$

$$\rho\left(\frac{\partial \overline{u}}{\partial t}+\overline{u}\frac{\partial \overline{u}}{\partial \overline{z}}+w\frac{\partial \overline{u}}{\partial r}\right)=-\frac{\partial \overline{p}}{\partial \overline{r}}+\mu\left(\frac{\partial^2 \overline{u}}{\partial \overline{z}^2}+\frac{\partial^2 \overline{u}}{\partial \overline{r}^2}+\frac{1}{\overline{r}}\frac{\partial \overline{u}}{\partial \overline{r}}\right)+\left(\frac{\partial S_{\overline{rz}}}{\partial \overline{z}}+\frac{S_{\overline{rr}}}{\overline{r}}+\frac{\partial S_{\overline{rr}}}{\partial \overline{r}}-\frac{S_{\theta\theta}}{\overline{r}}\right), \tag{11}$$

$$\rho\left(\frac{\partial w}{\partial t}+\overline{u}\frac{\partial w}{\partial \overline{z}}+w\frac{\partial w}{\partial r}\right)=-\frac{\partial \overline{p}}{\partial \overline{z}}+\mu\left(\frac{\partial^2 w}{\partial \overline{z}^2}+\frac{\partial^2 w}{\partial \overline{r}^2}+\frac{1}{\overline{r}}\frac{\partial w}{\partial \overline{r}}\right)+\left(\frac{\partial S_{\overline{zz}}}{\partial \overline{z}}+\frac{S_{\overline{zr}}}{\overline{r}}+\frac{\partial S_{\overline{zr}}}{\partial \overline{r}}\right), \tag{12}$$

$$\rho c_p\left(\frac{\partial T}{\partial t}+\overline{u}\frac{\partial T}{\partial \overline{z}}+w\frac{\partial T}{\partial r}\right)=k\left(\frac{\partial^2 T}{\partial \overline{z}^2}+\frac{\partial^2 T}{\partial \overline{r}^2}+\frac{1}{\overline{r}}\frac{\partial T}{\partial \overline{r}}\right)+S_{rr}\frac{\partial u}{\partial r}+S_{rz}\frac{\partial u}{\partial z}+S_{zr}\frac{\partial w}{\partial r}+S_{zz}\frac{\partial w}{\partial z}. \tag{13}$$

Using the dimensionless parameters,

$$\left.\begin{aligned} r* &= \frac{r}{R_0}, z^* = \frac{z}{\lambda}, w^* = \frac{w}{c}, u^* = \frac{u}{c\delta}, t^* = \frac{ct}{\lambda}, \\ \mathrm{Re} &= \frac{\rho a c}{\mu}, \delta = \frac{a}{\lambda}, H = \frac{T - T_0}{T_1 - T_0}, M = \frac{C - C_0}{C_1 - C_0}, \\ G_r &= \frac{\rho_f g \alpha a^2}{\mu_f c} T_0, p^* = \frac{a^2 p}{\mu_f c \lambda}, \phi_1 = \frac{b_1}{a_0}, \phi_2 = \frac{b_2}{a_0}. \end{aligned}\right\} \quad (14)$$

Employing nondimensional variables in equations (11)–(19) and using long wavelength and low Reynolds number approximation, the equations for peripheral and core region become as follows.

2.5.3. Peripheral Region in Dimensionless Form

$$0 = \frac{\partial \overline{p}}{\partial r}, \quad (15)$$

$$0 = -\frac{\partial \overline{p}}{\partial z} + \left(\frac{\partial^2 w_1}{\partial \overline{r}^2} + \frac{1}{\overline{r}}\frac{\partial w_1}{\partial \overline{r}}\right) - Da(w_1 + 1) + GrH_1 + BrM_1, \quad (16)$$

$$0 = \frac{\partial^2 H_1}{\partial \overline{r}^2} + \frac{1}{\overline{r}}\frac{\partial H_1}{\partial \overline{r}} + Br\left(\left(\frac{\partial w_1}{\partial r}\right)^2\right) + N_b\left(\frac{\partial M_1}{\partial \overline{r}}\frac{\partial H_1}{\partial \overline{r}}\right) + N_t\left(\left(\frac{\partial H_1}{\partial \overline{r}}\right)^2\right), \quad (17)$$

$$0 = N_b\left(\frac{\partial^2 M_1}{\partial \overline{r}^2} + \frac{1}{\overline{r}}\frac{\partial M_1}{\partial \overline{r}}\right) + N_t\left(\frac{\partial^2 H_1}{\partial \overline{r}^2} + \frac{1}{\overline{r}}\frac{\partial H_1}{\partial \overline{r}}\right). \quad (18)$$

2.5.4. Core Region in Dimensionless Form

$$0 = \frac{\partial \overline{p}}{\partial \overline{r}} \quad (19)$$

$$0 = -\frac{\partial \overline{p}}{\partial z} + \frac{\partial^2 w_2}{\partial \overline{r}^2} + \frac{1}{\overline{r}}\frac{\partial w_2}{\partial \overline{r}} + \frac{S_{\overline{zr}}}{\overline{r}} + \frac{\partial S_{\overline{zr}}}{\partial \overline{r}}, \quad (20)$$

$$0 = \frac{\partial^2 H_2}{\partial \overline{r}^2} + \frac{1}{\overline{r}}\frac{\partial H_2}{\partial \overline{r}} + Br\left(S_{zr}\frac{\partial w_2}{\partial r}\right), \quad (21)$$

$$Srr = We(1 + a)S_{zr}\frac{\partial w_2}{\partial r}, Szz = -We(1 - a)S_{zr}\frac{\partial w_2}{\partial r}, Srz = \frac{\eta/\mu_r \partial w_2/\partial r}{1 + We^2\left(1 - a^2\right)\left(\partial w_2/\partial r\right)^2}. \quad (22)$$

2.5.5. Boundary Conditions

$$r_2 = 1 + \phi_1 \cos 2\,\pi(z - t) + \phi_2 \cos 4\,\pi(z - t),$$

$$\begin{cases} w_1 = -1,\ H_1 = 0,\ @r = r_\epsilon \\ w_1 = w_2,\ H_1 = H_2,\ M = 0, \\ \dfrac{\eta/\mu_r \partial w_2/\partial r}{1 + We^2\left(1 - a^2\right)\left(\partial w_2/\partial r\right)^2} = \partial w_1/\partial r, \partial \mathrm{H}_1/\partial r = \dfrac{\partial H_2}{\partial r}, \quad @\, r = r_1 \\ w_2 = -1,\ H_2 = 1,\ M = 1,\ @\, r = r_2 \end{cases} \quad (23)$$

In addition to these constraints, we are also imposing the condition of compliant walls [14, 44, 45] on the outer surface which is defined as the continuity of stress at $r = r_2$:

$$\frac{\mathrm{d}p}{\mathrm{d}z} = E_1\frac{\partial^3 r_2}{\partial z^3} + E_2\frac{\partial^3 r_2}{\partial t^2 \partial z} + E_3\frac{\partial^2 r_2}{\partial t\,\partial z}. \quad (24)$$

By taking the Wissenburg number very small, i.e., $O(We^2)$, we get the following results from equation (18)–(21) and B.Cs. (22):

$$
\begin{aligned}
0 &= \frac{\partial \overline{p}}{\partial \overline{r}},\\
0 &= -\frac{\partial \overline{p}}{\partial z} + \left(1 + \frac{\eta}{\mu_r}\right)\frac{\partial^2 w_2}{\partial \overline{r}^2} + \frac{1}{\overline{r}}\left(1 + \frac{\eta}{\mu_r}\right)\frac{\partial w_2}{\partial \overline{r}},\\
0 &= \frac{\partial^2 H_2}{\partial \overline{r}^2} + \frac{1}{\overline{r}}\frac{\partial H_2}{\partial \overline{r}} + Br\frac{\eta}{\mu_r}\left(\frac{\partial w_2}{\partial r}\right)^2,\\
&\begin{cases}
w_1 = -1,\ H_1 = 0,\ atr = r_\epsilon\\
w_1 = w_2,\ H_1 = H_2,\ C = 0,\\
\dfrac{\eta}{\mu_r}\dfrac{\partial w_2}{\partial r} = \dfrac{\partial w_1}{\partial r},\ \dfrac{\partial H_1}{\partial r} = \dfrac{\partial H_2}{\partial r} \quad atr = r_1,\\
w_2 = -1,\ H_2 = 1,\ C = 1,\ atr = r_2.
\end{cases}
\end{aligned}
\tag{25}
$$

3. Solution Method

Mathematical modelling of the whole problem discussed above suggests that the two systems (peripheral and core regions) of coupled equations (21)–(27) are to be solved along with the coupled boundary limitations defined in equation (25). The system of the core region has been solved by an exact method, and the results are elaborated underneath:

$$
\begin{aligned}
H_2 &= C_6 + \frac{1}{4}\left(-\frac{C_{15}Brr^2\eta\left(C_{15}r^2\mu_r + 16C_1(\eta + \mu_r)\right)}{16(\eta + \mu_r)^2} + 4C_5 Log[r] - \frac{2BrC_1^2\eta Log[r]^2}{\mu_r}\right),\\
w_2 &= \frac{r^2\mu_r}{4(\eta + \mu_r)}C_{15} + C_2 + C_1 Log[r].
\end{aligned}
\tag{26}
$$

On the contrary, the system of the peripheral region cannot be solved exactly, so we adopted the scheme of perturbation (HPM) [46–48] in which the same linear operator is chosen for velocity, heat, and energy functions, i.e., $\mathscr{H} = \partial^2/\partial r^2 + 1/r\partial/\partial r$. After using the routine calculation of HPM, the final solutions have been composed in subsequent forms:

$$
\begin{pmatrix}
768C_{14}Nb + 3BrC_{15}r^2\begin{pmatrix} 32C_3(Nb + Nt) \\ +(Nb + 3Nt)G_1r^2 \end{pmatrix} + \\
\frac{1}{Log[r2] - Log[r\varepsilon]}\times \\
\begin{pmatrix}
128\,(\,(Nbt - nNqt)Log[r]^3(C_7Nb + \\
\left(BrC_3{}^2 + C_7{}^2Nt\right) \\
(Log[r_2] - Log[r_\varepsilon]) \\
+3Log[r]^2(C_7NbNt - \\
\left(C_{11}(Nb - Nt) - Nt\left(BrC_3^2 + C_7^2Nt\right)\right) \\
(Log[r_2] - Log[r_\varepsilon])) - 6NbLog[r_\varepsilon] + \\
6NbLog[r]1 + (C_{13}Log[r_2] \\
-C_{13}Log[r_\varepsilon])
\end{pmatrix}
\end{pmatrix}
$$

$$
\begin{aligned}
M_1 &= \frac{1}{768Nb}\times,\\
H_1 &= C_{12} + C_8 - \frac{1}{64}BrC_{15}r^2\left(16C_3 + C_{15}r^2\right) + \left(C_{11} + C_7\right)Log[r] + \frac{1}{2}Log[r]^2\\
&\quad \left(-BrC_3{}^2 + C_7\left(-C_7Nt + \frac{Nb}{-Log[r_2] + Log[r_\varepsilon]}\right)\right),\\
&\quad + \frac{r^2\begin{pmatrix} -\left(\left(-1 + C_3 - C_4\right)Da + \left(-C_7 + C_8\right)Gr\right)\\ \left(Log[r_2] - Log[r_\varepsilon]\right) + Br\left(1 + Log[r_\varepsilon]\right)\end{pmatrix}}{4\left(Log[r_2] - Log[r_\varepsilon]\right)} + \frac{1}{4}r^2Log[r]\left(C_3Da - C_7Gr + \frac{Br}{-Log[r_2] + Log[r_\varepsilon]}\right),\\
w_1 &= C_{10} + C_4 + \frac{C_{15}r^2}{4} + \frac{1/64Da\ C_{15}}{r^4} + C_3Log[r] + C_9Log[r],
\end{aligned}
\tag{27}
$$

where the constants C_n, $n = 1, 2, 3, \ldots 14$, are found by using B.Cs. (26) and are written in Appendix.

4. Results and Discussion

This section involves some graphical discussion based on the theoretical data achieved in the preceding section where we have collected analytical readings of observable sections of the study along with the compliant walls' phenomenon. To deal with this, we have captured some graphs of obtained analytical statistics of velocity, temperature, nanoparticles' fraction, and stream functions. Figures 2–8 reflect the sketches for the velocity field, Figures 9–13 for temperature, Figures 13–19 for nanoparticles, and Figures 20–23 for streamlines. Above mentioned graphs contain the behaviour of said profiles for both the peripheral and core regions. From these plots, we imagine that how a quantity varies against the including factor theoretically, and its matching with the physical aspects are also being stated.

4.1. Velocity Variation. Figure 2 contemplates the impact of the viscosity ratio parameter μ_r on the curves of velocity function w plotted along the radial coordinate r. After viewing this figure, we can state that velocity is showing direct variance with the rising impact of the said parameter. It is also to be mentioned here that blue lines carry the information of the peripheral portion while red lines convey the core region data. It is also noted that the peripheral region gives more parabolic curves than the core region and the velocity gets maximum in the central slab. On the contrary, the core region contains the more flatter curves which predict that velocity varies linearly with the radial coordinate and becomes minimum at the walls. Figure 3 depicts the variation of velocity for the parameter E_1 which accounts for mass per unit area. It can be started from the said graph that velocity is varying in increasing fashion when we increase the values of the factor E_1. It is also noted that very smooth and similar behaviour can be concluded in both regions. From Figures 4 and 5, we can visualize the effects of viscous damping force E_2 and flexure rigidity of the walls E_3, respectively, on the velocity envelop. It is found here that velocity is minimum at the static walls due to no slip at the boundaries, but it goes large in the middle lump of the domain between the peripheral and core regions. From Figure 6, it can be estimated that Brinkman number Br exerts a direct impact on velocity in the peripheral region, but the core region experiences no difference in velocity with the variation of the said factor which can be observed by a single bold red line in the figure. Figure 7 reveals the behaviour of fluid velocity under the variation of Darcy's number Da, and it can be suggested here that, in the peripheral region, velocity curves are suppressed with the increasing amount of Darcy's number, but on the core side, we receive no variance which suggests that porosity factors are only present on the outside walls and not on the inner surface of the channel. This variation can be physically justified as that due to pores on the peripheral region velocity of the fluid gets decreased as some molecules are resisted by the porous wall and gets sucked into the boundary causing the reduction in the flow speed. Figure 8 shows that velocity is depending on Grashof number Gr directly in the peripheral region, but there is no effect of the said factor in a core region which shows that the nanoparticles contribute significantly only in the mainstream of the flow.

4.2. Thermal Exchange. Figure 9 implies the variation of temperature distribution profile H under the variation of Brinkman number Br along the radial axis. It is measured from this plot that temperature goes direct with the Brinkman number. It is physically found from the graph that when we provide a large value to the Brinkman number, the heat is transferred to a large extent in the peripheral region, but in the core region, the variation remains direct but consistent. It is also found that maximum thermal exchange is reported at $r = 0 \cdot 3$, and then, after that, it starts decreasing throughout the domain. Figure 10 suggests that fluid dynamic viscosity factor η imposes inverse impact on the profile of temperature difference in the peripheral region which can be found in the graph through blue curves, but red curves are showing that, in the core region, heat is transferred at a very small rate which depicts that there is a very slight impact of fluid dynamic viscosity features in the core region regarding a change in temperature. When we look at Figure 11, we approach the fact that the Johnson–Segalman

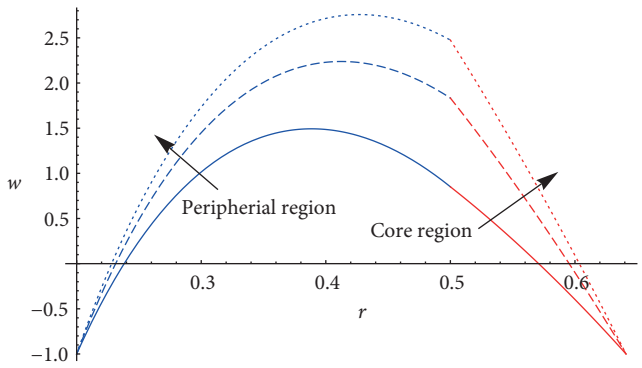

Solid line $\mu_r = 0.1$
Dashed line $\mu_r = 0.2$
Dotted line $\mu_r = 0.3$

Figure 2: Variation in velocity vs. radius of pipe for both fluids with changes in μ_r.

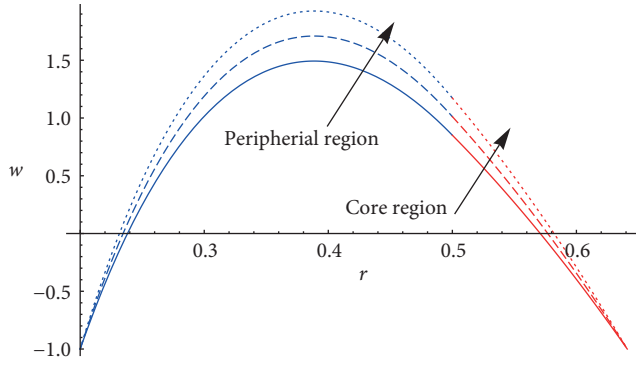

Solid line $E_1 = 0.1$
Dashed line $E_1 = 0.2$
Dotted line $E_1 = 0.3$

Figure 3: Variation in velocity vs. radius of pipe for both fluids with changes in E_1.

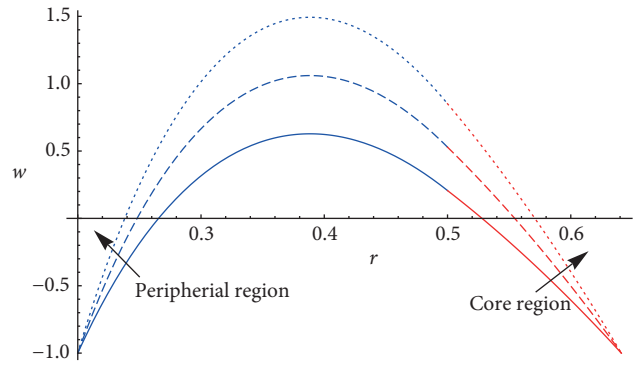

Solid line $E_2 = 0.5$
Dashed line $E_2 = 0.7$
Dotted line $E_2 = 0.9$

Figure 4: Variation in velocity vs. radius of pipe for both fluids with changes in E_2.

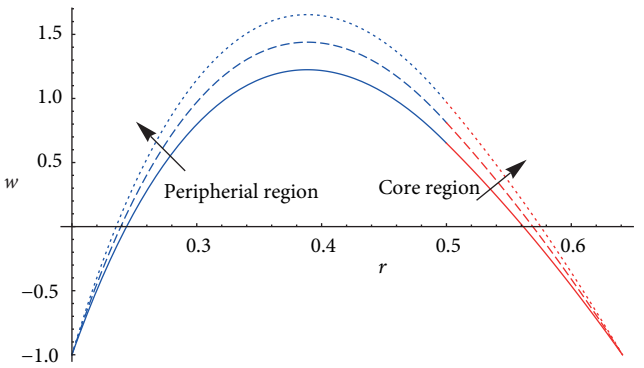

Solid line $E_3 = 0.1$
Dashed line $E_3 = 0.5$
Dotted line $E_3 = 0.9$

Figure 5: Variation in velocity vs. radius of pipe for both fluids with changes in E_3.

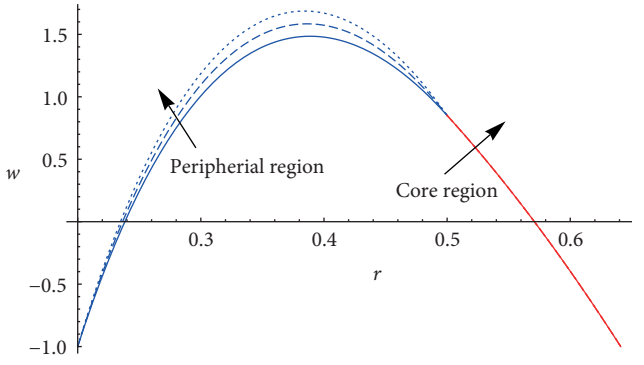

Bold line Br = 0.5
Dashed line Br = 5.0
Dotted line Br = 10

Figure 6: Variation in velocity vs. radius of pipe for both fluids with changes in Br.

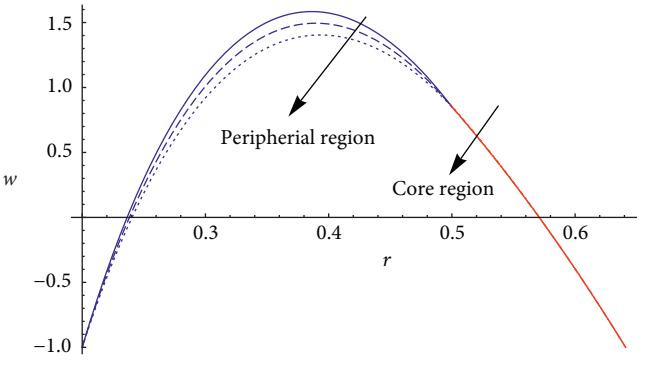

Solid line Da = 0.1
Dashed line Da = 4
Dotted line Da = 8

Figure 7: Variation in velocity vs. radius of pipe for both fluids with changes in Da.

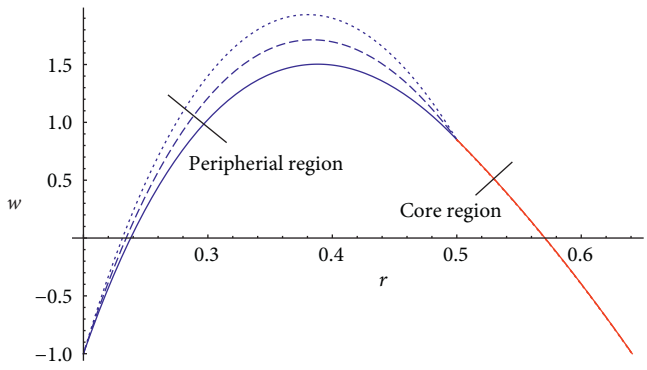

Solid line Gr = 0.10
Dashed line Gr = 05
Dotted line Gr = 10

Figure 8: Variation in velocity vs. radius of pipe for both fluids with changes in Gr.

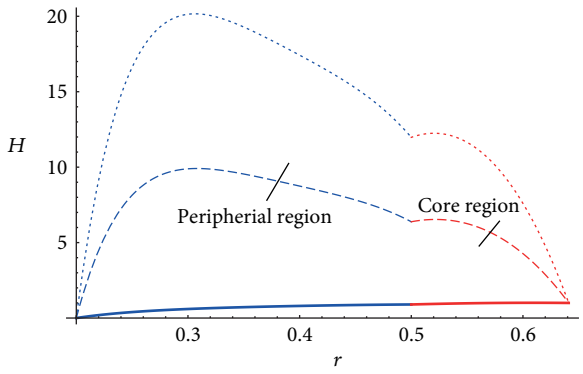

Bold line Br = 0.1
Dashed line Br = 5.0
Dotted line Br = 10

Figure 9: Variation in temperature vs. radius of pipe for both fluids with changes in Br.

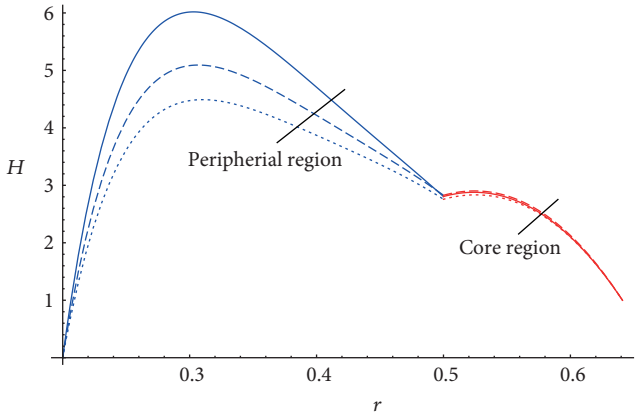

Bold line $\eta = 0.2$
Dashed line $\eta = 0.3$
Dotted line $\eta = 0.4$

Figure 10: Variation in temperature vs. radius of pipe for both fluids with changes in η.

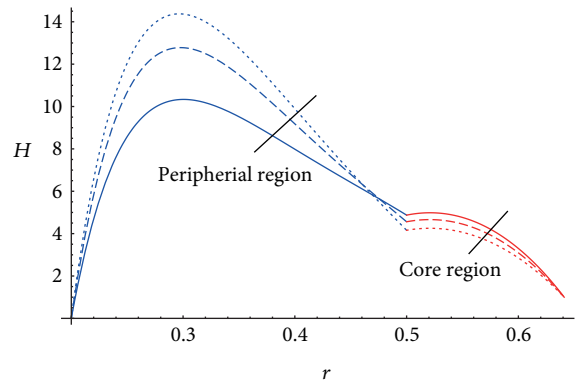

Solid line $\mu_r = 0.3$
Dashed line $\mu_r = 0.5$
Dotted line $\mu_r = 0.7$

Figure 11: Variation in temperature vs. radius of pipe for both fluids with changes in μ_r.

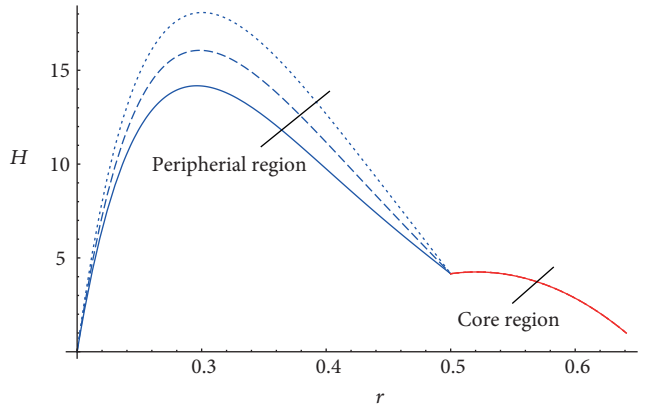

Bold line Nb = 0.3
Dashed line Nb = 5.0
Dotted line Nb = 10

Figure 12: Variation in temperature vs. radius of pipe for both fluids with changes in Nb.

fluid's variable viscosity μ_r is contributing to heat transfer indirect manner especially in the peripheral region which is in the region adjacent to the core region; also, in the whole core region, it puts inverse pressure on the thermal profile but at a lesser rate which results in decreasing the thermal transfer intensity. Figures 12 and 13 display the effects of Brownian diffusion Nb and thermophoresis diffusion Nt, accordingly on the heat exchange features. From both graphs, we receive almost the similar characteristics that are heat transfer curves rising in the peripheral region against both the factors, but there is no contribution of these two parameters in the core region as we have neglected their effects in the considered flow problem in the core region.

4.3. Nanoparticles' Phenomenon. As in the modelling section, we have considered the nanoparticles' phenomenon only in the core region, so we will here discuss the behaviour of nanoparticles' distribution only in the peripheral region.

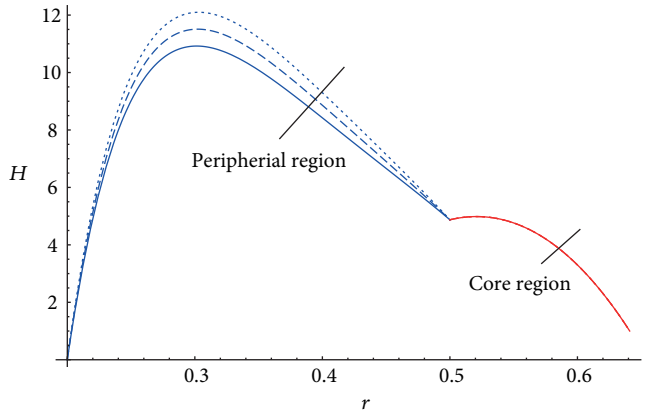

Bold line Nt = 0.3
Dashed line Nt = 0.5
Dotted line Nt = 0.7

Figure 13: Variation in temperature vs. radius of pipe for both fluids with changes in Nt.

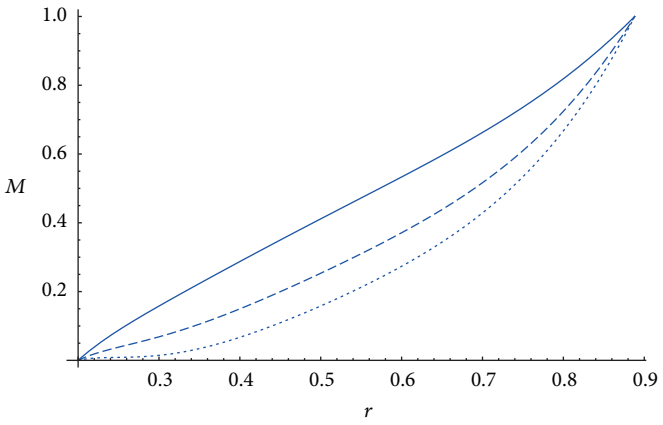

Solid line Br = 0.05
Dashed line Br = 0.10
Dotted line Br = 0.13

Figure 14: Variation in nanoparticles' concentration vs. radius of pipe for both fluids with changes in Br.

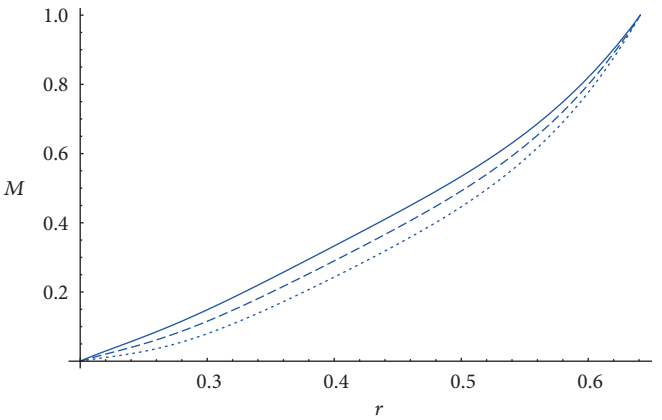

Solid line $E_1 = 0.1$
Dashed line $E_1 = 0.2$
Dotted line $E_1 = 0.3$

Figure 15: Variation in nanoparticles' concentration vs. radius of pipe for both fluids with changes in E_1.

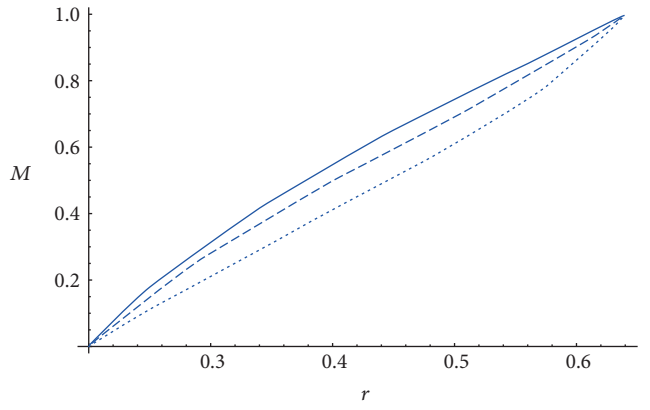

Solid line $E_2 = 0.1$
Dashed line $E_2 = 0.4$
Dotted line $E_2 = 0.7$

Figure 16: Variation in nanoparticles' concentration vs. radius of pipe for both fluids with changes in E_2.

Figure 14 discloses the effects of Brinkman number Br on the profile of nanoparticles' distribution M. It is noted here that Brinkman constant pushes back the nanoparticles' distribution. From Figure 15, it is concluded that rise in mass per unit factor E_1 results in decreasing nanoparticles' distribution which means that increase in mass of the compliant walls puts an inverse impact on the distribution of nanoparticles. The same behaviour is measured in front of viscous damping forces E_2 and flexure rigidity of the compliant walls E_3 which can be found in Figures 16 and 17, orderly, which implies the resistive effects of compliant walls on the nanoparticles' profile. From Figure 18, we can judge that viscosity μ_r shows inverse relation with the nanoparticles' flow rate, but in the domain $r > 0 \cdot 55$, almost constant characteristics are noted regarding the magnitude of nanoparticles' volume fraction. When we look at Figure 19, we come to the statement that Brownian diffusion factor Nb is directly proportional to the profile of M, but on the contrary, thermophoresis parameter Nt reflects opposite readings which can be visualized in Figure 20.

4.4. Streamlines' Discussion. Streamlines have been unveiled to discuss the flow sketches under the effects of some considerable features of the study. In Figure 21, the circulating bolus mechanism has been included for the factor E_1, and we have obtained that there are four portions, namely, 1st, 2nd, 3rd, and 4th quadrants taken in anticlockwise directions to discuss the flow pattern. In the first quadrant, the bolus volume increases for the value of $E_1 < 1$, but for $E_1 > 1$, the size is decreased, while in the 2nd portion, the size is continuously increasing. On the contrary, the 3rd and 4th quadrants reveal that bolus dimensions are decreasing. It is concluded here that an increase in mass/unit area of the

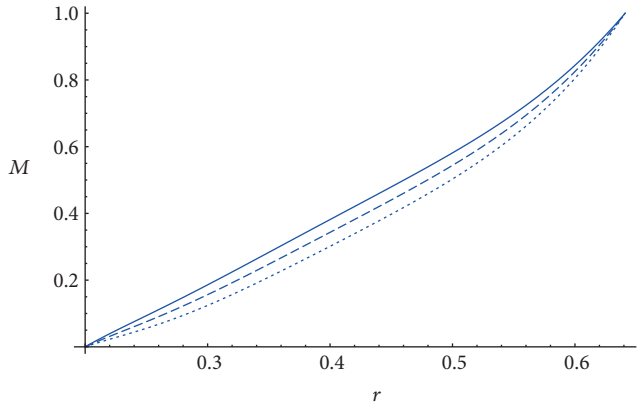

Solid line $E_3 = 0.1$
Dashed line $E_3 = 0.5$
Dotted line $E_3 = 0.9$

FIGURE 17: Variation in nanoparticles' concentration vs. radius of pipe for both fluids with changes in E_3.

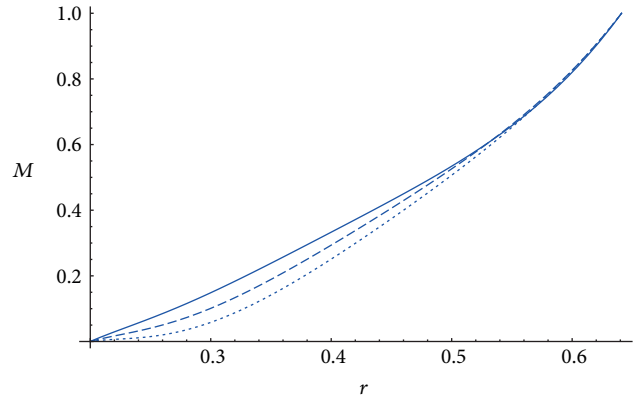

Solid line $\mu_r = 0.1$
Dashed line $\mu_r = 0.2$
Dotted line $\mu_r = 0.3$

FIGURE 18: Variation in nanoparticles' concentration vs. radius of pipe for both fluids with changes in μ_r.

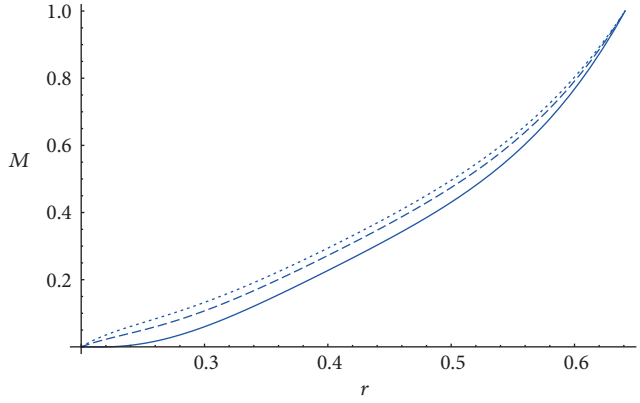

Solid line Nb = 0.5
Dashed line Nb = 0.7
Dotted line Nb = 0.9

FIGURE 19: Variation in nanoparticles' concentration vs. radius of pipe for both fluids with changes in *Nb*.

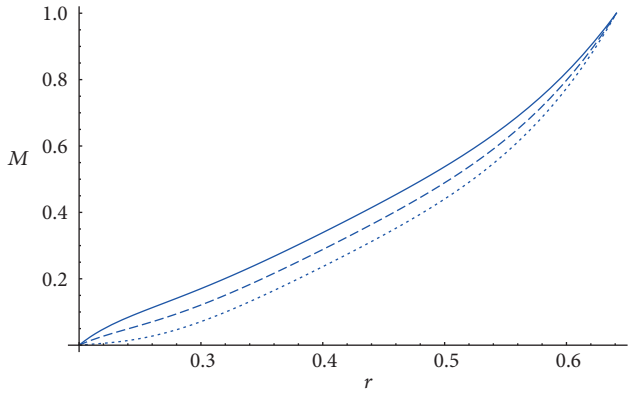

Solid line Nt = 0.1
Dashed line Nt = 0.2
Dotted line Nt = 0.3

Figure 20: Variation in nanoparticles' concentration vs. radius of pipe for both fluids with changes in Nt.

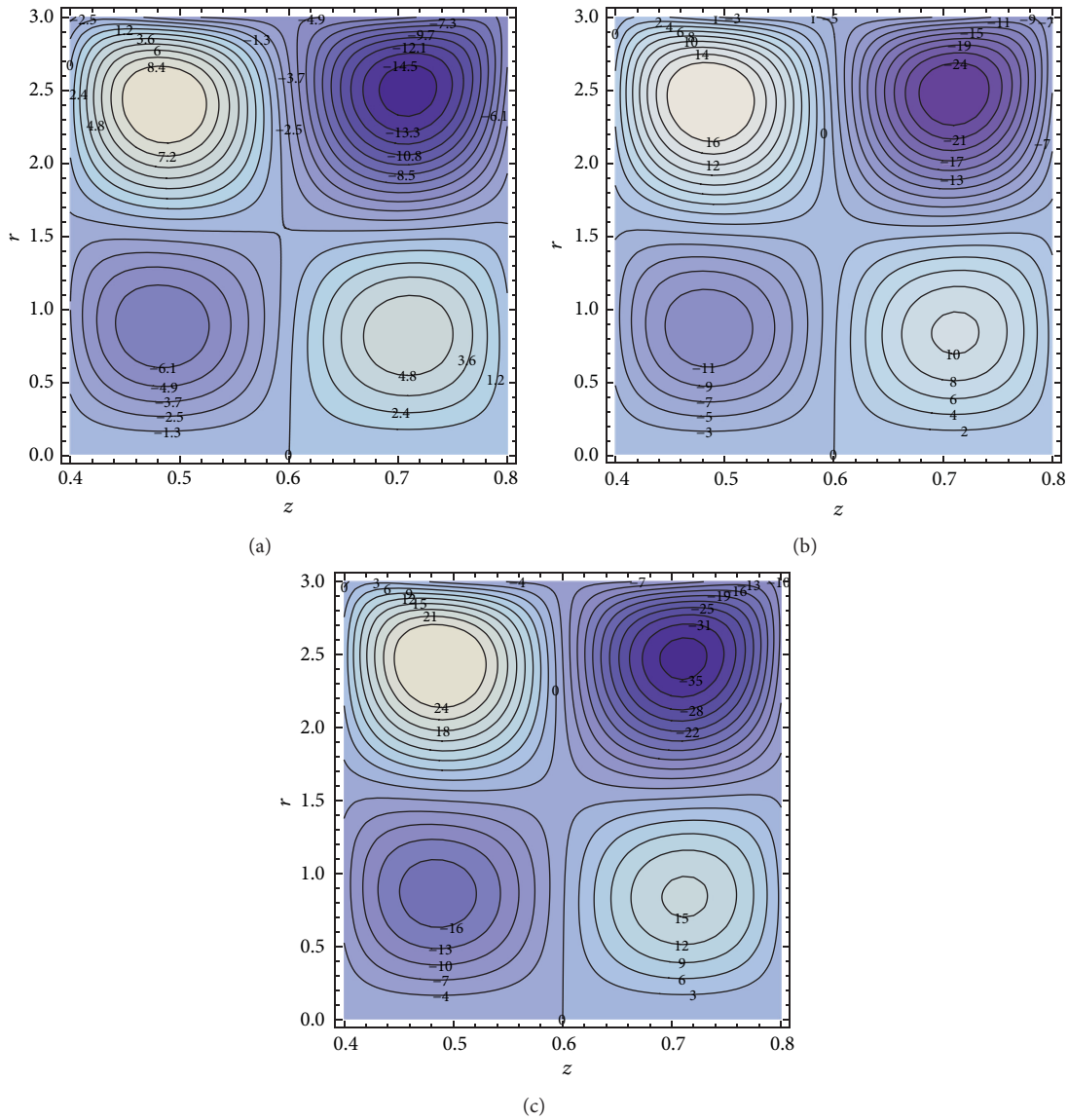

Figure 21: Variation in streamlines with E_1.

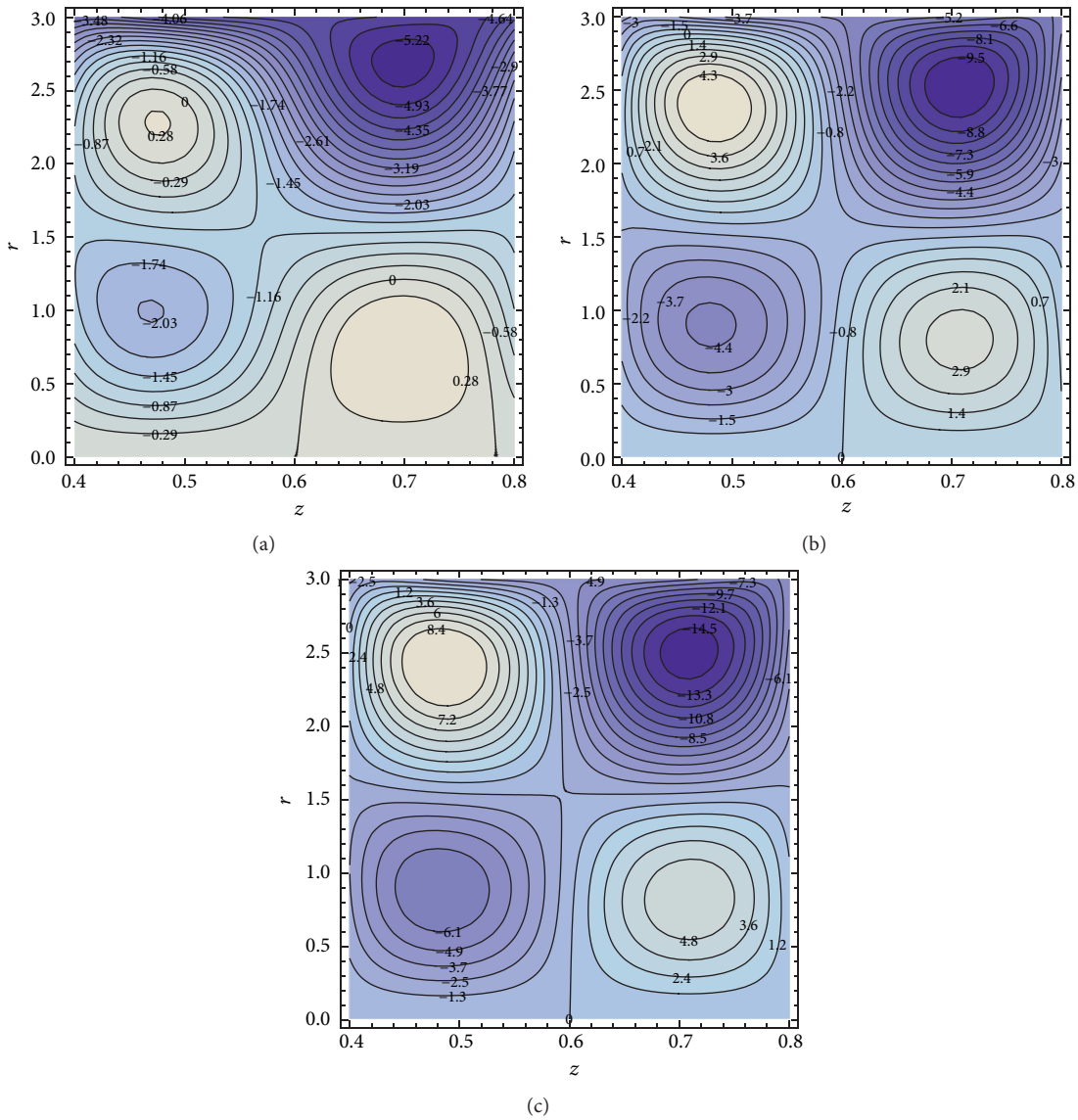

Figure 22: Variation in streamlines with E_2.

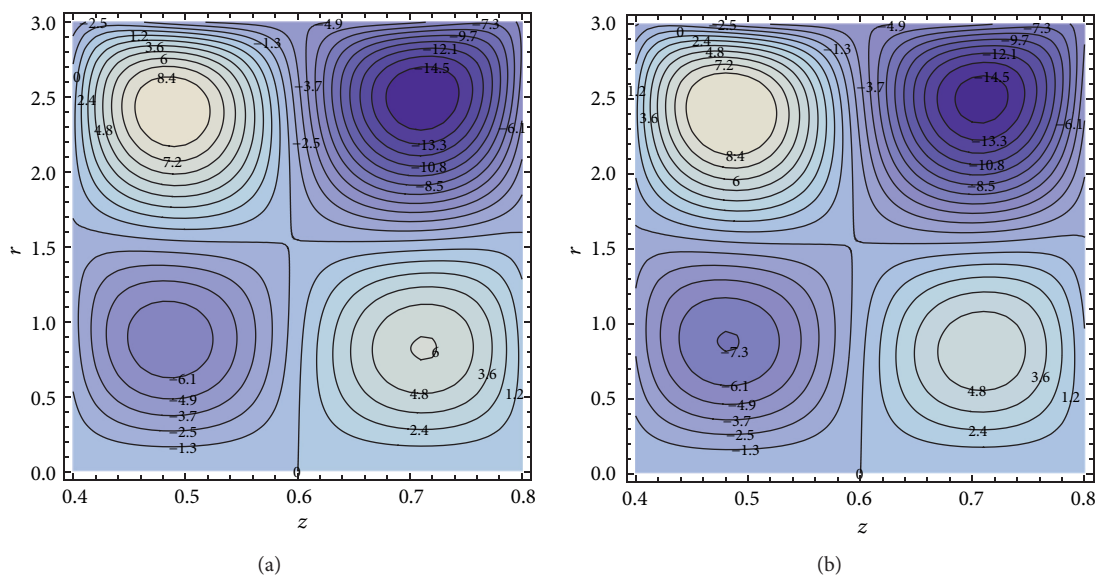

Figure 23: Continued.

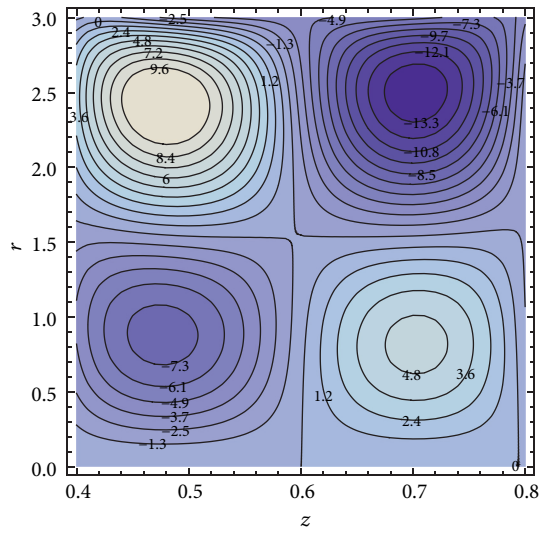

(c)

Figure 23: Variation in streamlines with E_3.

compliant walls puts pressure on the flow and in-response flow gets faster resulting decrease in the size of the boluses. Figure 22 describes the variation of stream boluses by the increasing variety of viscous damping force E_2. It can be decided here that most of the size of the space of the circulating contours is increasing, resulting in decrease in the flow rate which may be due to the large viscous damping forces pressure producing large boluses due to the lesser speed of the fluid. Figure 23 directs that in the 1st and 3rd quadrant, more boluses are produced with relatively lesser sizes for $E_3 < 1$, but for $E_3 > 1$, the situation is the opposite. On the contrary, the boluses in the rest of the quadrants are broken with a large magnitude of the parameter resulting in a decrease in the number of contours.

5. Concluding Remarks

Currently, we have discovered the theoretical analysis of the bi-layered flow of Johnson–Segalman/nanofluid with peristaltic phenomenon through an infinitely long circular axis-symmetric co-centric cylinder having flexible outer walls under the constraints of long wavelength and low Reynolds number. The flow has been observed in two layers, namely, peripheral and core regions. The unknown quantities of the core region have been achieved by exact solutions, but the peripheral region has been tackled by HPM. The developed analytic solutions have been sketched on Mathematica and discussed descriptively. From the above whole study, we collected the following important points:

(i) The velocity is an increasing function of fluid viscosity μ_r in both the regions, but the profile is much flatter in the core region as compared to the peripheral region, depicting the result that fluid viscosity affects the flow speed significantly in the peripheral region than the core region.

(ii) It is finalized that compliant walls are executing the same sort of effect on the flow characteristics in both the peripheral and core portions, and overall, the flow speeds up due to walls' compliance.

(iii) It should be added that velocity is enhanced due to the large intensity of Brinkman number and Grashof number which is not in the case of wall's porosity effects.

(iv) It can be stated that the Brinkman number increases the rate of thermal transfer in both the regions.

(v) It can also be placed here that the heat transfer rate is decreasing with increasing fluid viscosity η in the peripheral region.

(vi) It is found that nanoparticles' distribution goes backwards due to compliant walls, fluid's viscosity, Brinkman number, and thermophoresis factor but moves forward by the Brownian diffusion.

(vii) Due to the large mass per unit area of the compliant walls, the circulating contours are squeezed.

More research on the topic can be made by taking different types of nanoparticles and by considering their affective properties; also, the effects of magnetic field and electro-osmotic mechanism can be described in future. The study can be made by inclusion of electro-osmotic effects as well.

Appendix

A. List of Coefficients

$$C_1 = \frac{C_{15}\mu_r\left(-r_1{}^2\eta - r_2{}^2\mu_r + r_\varepsilon{}^2(\eta+\mu_r) + 2r_1{}^2\mu_r(Log[r_1] - Log[r_\varepsilon])\right)}{4(\eta+\mu_r)((\eta-\mu_r)Log[r_1] + \mu_r Log[r_2] - \eta Log[r_\varepsilon])}, \tag{A.1}$$

$$C_2 = \frac{1}{4}\left(-4 - \frac{C_{15}r_2^2\mu_r}{\eta+\mu_r} + \frac{C_{15}\mu_r Log[r_2]\left(r_1{}^2\eta + r_2{}^2\mu_r - r_\varepsilon{}^2(\eta+\mu_r) + 2r_1{}^2\mu_r(-Log[r_1] + Log[r_\varepsilon])\right)}{(\eta+\mu_r)((\eta-\mu_r)Log[r_1] + \mu_r Log[r_2] - \eta Log[r_\varepsilon])}\right), \tag{A.2}$$

$$C_3 = \frac{C_{15}\left(\eta\left(-r_1{}^2\eta - r_2{}^2\mu_r + r_\varepsilon{}^2(\eta+\mu_r)\right) + 2r_1{}^2\mu_r{}^2(\mathrm{Log}[r_1] - \mathrm{Log}[r_2])\right)}{4(\eta+\mu_r)((\eta-\mu_r)\mathrm{Log}[r_1] + \mu_r\mathrm{Log}[r_2] - \eta\mathrm{Log}[r_\varepsilon])}, \tag{A.3}$$

$$C_4 = \frac{1}{4}\left(-4 - C_{15}r_\varepsilon{}^2 + \frac{C_{15}\left(\eta\left(r_1{}^2\eta + r_2{}^2\mu_r - r_\varepsilon{}^2(\eta+\mu_r)\right) + 2r_1{}^2\mu_r{}^2(-\mathrm{Log}[r_1] + \mathrm{Log}[r_2])\right)\mathrm{Log}[r_\varepsilon]}{(\eta+\mu_r)((\eta-\mu_r)\mathrm{Log}[r_1] + \mu_r\mathrm{Log}[r_2] - \eta\mathrm{Log}[r_\varepsilon])}\right), \tag{A.4}$$

$$C_5 = \begin{pmatrix} \mu_r\left(16\left(4 + BrC_1C_{15}\left(-r_1^2 + r_2^2\right)\right)\eta^2 + \begin{pmatrix} 128 - BrC_{15}(r_1 - r_2)(r_1 + r_2) \\ \left(16C_1 + C_{15}\left(r_1^2 + r_2^2\right)\right) \end{pmatrix}\eta\mu_r + 64\mu_r^2\right) + \\ 4Br\eta(8C_1^2(\eta+\mu_r)^2 Log[r_1]^2 + 8C_1^2(\eta+\mu_r)^2 Log[r_2]^2 - C_{15}r_1^2\mu_r\left(C_{15}r_1^2\mu_r + 8C_1(\eta+\mu_r)\right)\mathrm{Log}[r_\varepsilon]\mathrm{Log}[r_1], \\ \left(C_{15}r_1^2\mu_r\left(C_{15}r_1^2\mu_r + 8C_1(\eta+\mu_r)\right) - \frac{16C_1^2}{\left(64\mu_r(\eta+\mu_r)^2(\mathrm{Log}[r_2] - \mathrm{Log}[r_\varepsilon])\right)}\right. \end{pmatrix} \tag{A.5}$$

$$C_6 = 1 + \frac{Br\eta Log[r_2]^2 C_1^2}{2\mu_r} + \frac{r_2^2 Br\eta C_1 C_{15}}{4(\mu_r+\eta)} + \frac{r_2^4\mu_r Br\eta C_{15}^2}{64(\mu_r+\eta)^2} + Log[r_2]\left(-r_1\left(\frac{Br\eta Log[r_1]C_1^2}{r_1\mu_r} + \frac{r_1 Br\eta C_1 C_{15}}{2(\mu_r+\eta)} + \frac{r_1^3\mu_r Br\eta C_{15}^2}{16(\mu_r+\eta)^2}\right) + \frac{\left(-(-Log[r_1] + Log[r_2])\left(Br\eta Log[r_1]C_1^2/r_1\mu_r + r_1 Br\eta C_1C_{15}/2(\mu_r+\eta) + r_1^3\mu_r Br\eta C_{15}^2/16(\mu_r+\eta)^2\right) - \left(\begin{matrix} -1 + Br\eta Log[r_1]^2C_1^2/2\mu_r - Br\eta Log[r_2]^2C_1^2/2\mu_r + r_1^2 Br\eta C_1C_{15}/4(\mu_r+\eta) - \\ r_2^2 Br\eta C_1C_{15}/4(\mu_r+\eta) + r_1^4\mu_r Br\eta C_{15}^2/64(\mu_r+\eta)^2 - r_2^4\mu_r Br\eta C_{15}^2/64(\mu_r+\eta)^2 \end{matrix}\right)/r_1\right)}{(-Log[r_2]/r_1 + Log[r_\varepsilon]/r_1)}, \tag{A.6}$$

$$C_7 = -\frac{\left(\begin{matrix} -(-Log[r_1] + Log[r_2])\left(Br\eta Log[r_1]C_1^2/r_1\mu_r + r_1 Br\eta C_1C_{15}/2(\mu_r+\eta) + r_1^3\mu_r Br\eta C_{15}^2/16(\mu_r+\eta)^2\right) - \\ \left(\begin{matrix} -1 + Br\eta Log[r_1]^2C_1^2/2\mu_r - Br\eta Log[r_2]^2C_1^2/2\mu_r + r_1^2 Br\eta C_1C_{15}/4(\mu_r+\eta) - \\ r_2^2 Br\eta C_1C_{15}/4(\mu_r+\eta) + r_1^4\mu_r Br\eta C_{15}^2/64(\mu_r+\eta)^2 - r_2^4\mu_r Br\eta C_{15}^2/64(\mu_r+\eta)^2 \end{matrix}\right)/r_1 \end{matrix}\right)}{-Log[r_2]/r_1 + Log[r_\varepsilon]/r_1}, \tag{A.7}$$

$$C_8 = \frac{Log[r_\varepsilon]\left(\begin{matrix} -(-Log[r_1] + Log[r_2])\left(Br\eta Log[r_1]C_1^2/r_1\mu_r + r_1 Br\eta C_1C_{15}/2(\mu_r+\eta) + r_1^3\mu_r Br\eta C_{15}^2/16(\mu_r+\eta)^2\right) - \\ \left(\begin{matrix} -1 + Br\eta Log[r_1]^2C_1^2/2\mu_r - Br\eta Log[r_2]^2C_1^2/2\mu_r + r_1^2 Br\eta C_1C_{15}/4(\mu_r+\eta) - \\ r_2^2 Br\eta C_1C_{15}/4(\mu_r+\eta) + r_1^4\mu_r Br\eta C_{15}^2/64(\mu_r+\eta)^2 - r_2^4\mu_r Br\eta C_{15}^2/64(\mu_r+\eta)^2 \end{matrix}\right)/r_1 \end{matrix}\right)}{-Log[r_2]/r_1 + Log[r_\varepsilon]/r_1}, \tag{A.8}$$

$$C_9 = \frac{1}{64(Log[r_1] - Log[r_\varepsilon])(-Log[r_2] + Log[r_\varepsilon])} \cdot \left(\begin{matrix} 16(-r_1^2 BrLog[r_1] + (r_1 - r_\varepsilon)(r_1 + r_\varepsilon)(Br + Da\ Log[r_2]) + \left(r_1^2(Br - Da) + r_\varepsilon^2 Da\right)Log[r_\varepsilon] + (Log[r_2] - Log[r_\varepsilon]) \\ \left(16\left(Da\left(-r_1^2 + r_\varepsilon^2 + r_1^2 Log[r_1] - r_\varepsilon^2 Log[r_\varepsilon]\right)C_3 + (r_1 - r_\varepsilon)(r_1 + r_\varepsilon)Da\ C_4 + Gr\left(r_1^2 - r_\varepsilon^2 - r_1^2 Log[r_1] + r_\varepsilon^2 Log[r_\varepsilon]\right)C_7 + \left(-r_1^2 + r_\varepsilon^2\right)GrC_8\right) + \left(r_1^4 - r_\varepsilon^4\right)Da\ C_{15}\right) \end{matrix}\right), \tag{A.9}$$

$$C_9 = \frac{1}{64\left(Log[r_1] - Log[r_\varepsilon]\right)\left(-Log[r_2] + Log[r_\varepsilon]\right)} \cdot \Big(16\Big(-r_1^2 Log[r_\varepsilon]\left(Br + Da\ Log[r_2]\right) + (Br - Da)Log[r_\varepsilon]\Big) + Log[r_1]\Big(r_\varepsilon^2 Da\left(Log[r_2] - Log[r_\varepsilon]\right) + Br\Big(r_\varepsilon^2 + r_1^2 Log[r_\varepsilon]\Big)\Big)\Big) + \left(Log[r_2] - Log[r_\varepsilon]\right) \left(16\begin{pmatrix} Da\left(-r_\varepsilon^2 Log[r_1] - \left(r_1^2 + \left(-r_1^2 + r_\varepsilon^2\right)Log[r_1]\right)Log[r_\varepsilon]\right)C_3 + Da\left(r_\varepsilon^2 Log[r_1] - r_1^2 Log[r_\varepsilon]\right)C_4 \\ +Gr\left(-r_1^2 Log[r_\varepsilon] + Log[r_1] + \left(r_\varepsilon^2 + (r_1 - r_\varepsilon)(r_1 + r_\varepsilon)Log[r_\varepsilon]\right)\right)C_7 + Gr\left(-r_\varepsilon^2 Log[r_1] + r_1^2 Log[r_\varepsilon]\right)C_3 \end{pmatrix} + Da\left(r_\varepsilon^4 Log[r_1] - r_1^4 Log[r_\varepsilon]\right)C_{15}\Big), \tag{A.10}$$

$$C_{11} = \frac{\begin{pmatrix} -32\left(Log[r_1]^2 - Log[r_\epsilon]^2\right)\left(NbC_7 + \left(Log[r_2] - Log[r_\epsilon]\right)\left(BrC_3^2 + NtC_7^2\right)\right) + \\ 16(r_1 - r_\epsilon)(r_1 + r_\epsilon)Br\left(-Log[r_2] + Log[r_\epsilon]\right)C_3C_{15} + \left(r_1^4 - r_\epsilon^4\right)Br\left(-Log[r_2] + Log[r_\epsilon]\right)C_{15}^2 \end{pmatrix}}{64\left(Log[r_1] - Log[r_\epsilon]\right)\left(-Log[r_2] + Log[r_\epsilon]\right)}, \tag{A.11}$$

$$C_{12} = \frac{1}{64\left(Log[r_1] - Log[r_\varepsilon]\right)\left(-Log[r_2] + Log[r_\varepsilon]\right)} \cdot \begin{pmatrix} 32Log[r_1]\left(Log[r_1] - Log[r_\varepsilon]\right)Log[r_\varepsilon] \\ \left(NbC_7 + \left(Log[r_2] - Log[r_\varepsilon]\right)\left(BrC_3^2 + NtC_7^2\right)\right) + 16Br\left(Log[r_2] - Log[r_\varepsilon]\right) \\ \left(-r_\varepsilon^2 Log[r_1] + r_1^2 Log[r_\varepsilon]\right)C_3C_{15} + Br\left(Log[r_2] - Log[r_\varepsilon]\right)\left(-r_\varepsilon^4 Log[r_1] + r_1^4 Log[r_\varepsilon]\right)C_{15}^2 \end{pmatrix}, \tag{A.12}$$

$$C_{13} = \frac{1}{768Nb\left(Log[r_2] - Log[r_\epsilon]\right)} \cdot \begin{pmatrix} 128Br\left(-3NtLog[r_2]^2 + (-Nb + Nt)Log[r_2]^3 + Log[r_\epsilon]^2\left(3Nt + (Nb - Nt)Log[r_\epsilon]\right)\right) \\ C_3^2 - 128\Big((Nb - Nt)Log[r_2]^2 + Log[r_2]\left(3Nt + (Nb - Nt)Log[r_\epsilon]\right) + Log[r_\epsilon]\left(3Nt + (Nb - Nt)Log[r_\epsilon]\right)\Big) \\ C_7\left(Nb + Nt\left(Log[r_2] - Log[r_\epsilon]\right)C_7\right) + 384\left(Nb - Nt\right)\left(Log[r_2]^2 - Log[r_\epsilon]^2\right) \\ C_{11} - 96\left(r_2 - r_\epsilon\right)\left(r_2 + r_\epsilon\right)Br\left(Nb + Nt\right)C_3C_{15} - 3\left(r_2^4 - r_\epsilon^4\right)Br\left(Nb + 3Nt\right)C_{15}^2 \end{pmatrix}, \tag{A.13}$$

$$C_{14} = -\frac{1}{768Nb\left(Log[r_2] - Log[r_\epsilon]\right)} \cdot \begin{pmatrix} 128BrLog[r_2]\left(Log[r_2] - Log[r_\epsilon]\right)Log[r_\epsilon]\left(-3Nt - (Nb - Nt)\left(Log[r_2] + Log[r_\epsilon]\right)\right) \\ C_3^2 - 128Log[r_2]Log[r_\epsilon]\left(3Nt + (Nb - Nt)\left(Log[r_2] + Log[r_\epsilon]\right)\right) \\ C_7\left(Nb + Nt\left(Log[r_2] - Log[r_\epsilon]\right)C_7\right) + 3\left(-Nb + Nt\right)\left(Log[r_2] - Log[r_\epsilon]\right)C_{11}) + \\ 96Br\left(Nb + Nt\right)\left(r_\epsilon^2 Log[r_2] - r_2^2 Log[r_\epsilon]\right)C_3C_{15} + 3Br\left(Nb + 3Nt\right)\left(r_\epsilon^4 Log[r_2] - r_2^4 Log[r_\epsilon]\right)C_{15}^2 \end{pmatrix}, \tag{A.14}$$

$$C_{15} = E_3\left(4\pi^2\phi_1 Cos[2\pi(-t + z)] + 16\pi^2\phi_2 Cos[4\pi(-t + z)]\right) + E_1\left(8\pi^3\phi_1 Sin[2\pi(-t + z)] + 64\pi^3\phi_2 Sin[4\pi(-t + z)]\right) + E_2\left(8\pi^3\phi_1 Sin[2\pi[-t + z]] + 64\pi^3\phi_2 Sin[4\pi(-t + z)]\right). \tag{A.15}$$

Data Availability

This is a theoretical study and there are no associated data. Numerical codes can be obtained from the corresponding author upon request.

Conflicts of Interest

The authors declare that they have no conflicts of interest.

References

[1] Y. C. Fung and C. S. Yih, "Peristaltic transport," *Journal of Applied Mechanics*, vol. 35, no. 4, pp. 669–675, 1968.

[2] K. R. Diller, "Modeling of bioheat transfer processes at high and low temperatures," *Advances in Heat Transfer*, vol. 22, pp. 157–357, 1992.

[3] T. W. Latham, *Fluid Motions in a Peristaltic Pump*, Doctoral dissertation, Massachusetts Institute of Technology, Massachusetts, USA, 1966.

[4] T. Hayat, N. Aslam, M. I. Khan, M. I. Khan, and A. Alsaedi, "Physical significance of heat generation/absorption and Soret effects on peristalsis flow of pseudoplastic fluid in an inclined channel," *Journal of Molecular Liquids*, vol. 275, pp. 599–615, 2019.

[5] Q. Afzal, S. Akram, R. Ellahi, S. M. Sait, and F. Chaudhry, "Thermal and concentration convection in nanofluids for peristaltic flow of magneto couple stress fluid in a nonuniform channel," *Journal of Thermal Analysis and Calorimetry*, vol. 144, no. 6, pp. 2203–2218, 2021.

[6] K. S. Mekheimer and Y. Abd elmaboud, "Peristaltic Transport through Eccentric Cylinders: Mathematical Model," *Applied Bionics and Biomechanics*, vol. 10, no. 1, pp. 19–27, 2013.

[7] Z. Nisar, T. Hayat, A. Alsaedi, and B. Ahmad, "Wall properties and convective conditions in MHD radiative peristalsis flow of Eyring–Powell nanofluid," *Journal of Thermal Analysis and Calorimetry*, vol. 144, no. 4, pp. 1199–1208, 2021.

[8] O. U. Mehmood, A. A. Qureshi, H. Yasmin, and S. Uddin, "Thermo-mechanical analysis of non Newtonian peristaltic mechanism: Modified heat flux model," *Physica A: Statistical Mechanics and Its Applications*, vol. 550, Article ID 124014, 2020.

[9] M. Y. Jaffrin and A. H. Shapiro, "Peristaltic pumping," *Annual Review of Fluid Mechanics*, vol. 3, no. 1, pp. 13–37, 1971.

[10] A. Zeeshan, A. Riaz, and F. Alzahrani, *Electrophoresis*, National Human Genome Research Institute, Mary land, USA, 2021.

[11] D. Tripathi, A. Sharma, and O. A. Bég, "Joule heating and buoyancy effects in electro-osmotic peristaltic transport of aqueous nanofluids through a microchannel with complex wave propagation," *Advanced Powder Technology*, vol. 29, no. 3, pp. 639–653, 2018.

[12] K. Javid, N. Ali, and Z. Asghar, "Numerical Simulation of The Peristaltic Motion of a Viscous Fluid Through a Complex Wavy Non-Uniform Channel With The Magneto-Hydrodynamic Effects," *Physica Scripta*, vol. 94, no. 11, Article ID 115226, 2019.

[13] D. Tripathi, R. Jhorar, O. A. Bég, and A. Kadir, "Electro-magneto-hydrodynamic peristaltic pumping of couple stress biofluids through a complex wavy micro-channela," *Journal of Molecular Liquids*, vol. 236, p. 358, 2017.

[14] M. M. Bhatti, R. Ellahi, A. Zeeshan, M. Marin, and N. Ijaz, "Numerical study of heat transfer and Hall current impact on peristaltic propulsion of particle-fluid suspension with compliant wall properties," *Modern Physics Letters B*, vol. 33, no. 35, Article ID 1950439, 2019.

[15] G. Bugliarello and J. Sevilla, "Velocity distribution and other characteristics of steady and pulsatile blood flow in fine glass tubes," *Biorheology*, vol. 7, no. 2, pp. 85–107, 1970.

[16] V. P. Srivastava, "A theoretical model for blood flow in small vessels," *Applications and Applied Mathematics: An International Journal (AAM)*, vol. 2, no. 1, p. 5, 2007.

[17] L. M. Srivastava and V. P. Srivastava, "Peristaltic transport of a two-layered model of physiological fluid," *Journal of Biomechanics*, vol. 15, no. 4, p. 257, 1982.

[18] S. L. Weinberg, E. C. Eckstein, and A. H. Shapiro, "An experimental study of peristaltic pumping," *Journal of Fluid Mechanics*, vol. 49, no. 3, p. 461, 1971.

[19] J. C. Misra and S. K. Pandey, "Peristaltic transport of blood in small vessels: Study of a mathematical model," *Computers & Mathematics with Applications*, vol. 43, no. 8-9, p. 1183, 2002.

[20] K. S. S. Vajravelu and R. Saravana, "Influence of velocity slip and temperature jump conditions on the peristaltic flow of a Jeffrey fluid in contact with a Newtonian fluid," *Applied Mathematics and Nonlinear Sciences*, vol. 2, no. 2, p. 429, 2017.

[21] N. Ali, S. Hussain, and K. Ullah, "Theoretical analysis of two-layered electro-osmotic peristaltic flow of FENE-P fluid in an axisymmetric tube," *Physics of Fluids*, vol. 32, no. 2, Article ID 023105, 2020.

[22] N. Ali, S. Hussain, K. Ullah, and O. A. Bég, "Mathematical modelling of two-fluid electro-osmotic peristaltic pumping of an Ellis fluid in an axisymmetric tube," *The European Physical Journal Plus*, vol. 134, p. 141, 2019.

[23] C. Rajashekhar, G. Manjunatha, K. V. Prasad, B. B. Divya, and H. Vaidya, "Peristaltic transport of two-layered blood flow using Herschel–Bulkley Model," *Cogent Engineering*, vol. 5, no. 1, Article ID 1495592, 2018.

[24] D. Tripathi, A. Borode, R. Jhorar, O. A. Bég, and A. K. Tiwari, "Computer modelling of electro-osmotically augmented three-layered microvascular peristaltic blood flow," *Microvascular Research*, vol. 114, pp. 65–83, 2017.

[25] S. Shubham, N. Jain, V. Gupta, S. Mohan, M. M. Ariffin, and A. Ahmadian, "Identify glomeruli in human kidney tissue images using a deep learning approach," *Soft Computing*, 2021.

[26] P. J. Cook, R. Doll, and S. A. Fellingham, "A mathematical model for the age distribution of cancer in man," *International Journal of Cancer*, vol. 4, no. 1, pp. 93–112, 1969.

[27] E. Ackerman, J. W. Rosevear, and W. F. McGuckin, "A Mathematical Model of the Glucose-tolerance test," *Physics in Medicine & Biology*, vol. 9, no. 2, p. 203, 1964.

[28] N. Jain, S. Jhunthra, H. Garg et al., "Prediction modelling of COVID using machine learning methods from B-cell dataset," *Results in physics*, vol. 21, Article ID 103813, 2021.

[29] V. Gupta, N. Jain, P. Katariya et al., "An Emotion Care Model using Multimodal Textual Analysis on COVID-19," *Chaos, Solitons & Fractals*, vol. 144, Article ID 110708, 2021.

[30] A. I. Dobrolyubov and G. Douchy, "Peristaltic Transport as the Travelling Deformation Waves," *Journal of Theoretical Biology*, vol. 219, no. 1, p. 55, 2002.

[31] I. Waini, A. Ishak, T. Groşan, and I. Pop, "Mixed convection of a hybrid nanofluid flow along a vertical surface embedded in a porous medium," *International Communications in Heat and Mass Transfer*, vol. 114, Article ID 104565, 2020.

[32] T. Hayat, F. Haider, A. Alsaedi, and B. Ahmad, "Unsteady flow of nanofluid through porous medium with variable characteristics," *International Communications in Heat and Mass Transfer*, vol. 119, Article ID 104904, 2020.

[33] A. Yasin, N. Ullah, S. Saleem, S. Nadeem, and A. Al-Zubaidi, "Impact of uniform and non-uniform heated rods on free convective flow inside a porous enclosure: Finite element analysis," *Physica Scripta*, vol. 96, no. 8, Article ID 085203, 2021.

[34] U. Nazir, M. A. Sadiq, and M. Nawaz, "Non-Fourier thermal and mass transport in hybridnano-Williamson fluid under chemical reaction in Forchheimer porous medium," *International Communications in Heat and Mass Transfer*, vol. 127, Article ID 105536, 2021.

[35] T. Abbas, B. Ahmad, A. Majeed, T. Muhammad, and M. Ismail, "Numerical Investigations of Radiative Flow of Viscous Fluid Through Porous Medium," *Journal of Magnetics*, vol. 26, no. 3, p. 277, 2021.

[36] S. Nadeem, N. Abbas, and M. Y. Malik, "Inspection of hybrid based nanofluid flow over a curved surface," *Computer Methods and Programs in Biomedicine*, vol. 189, Article ID 105193, 2020.

[37] A. Riaz, R. Ellahi, and S. M. Sait, "Role of hybrid nanoparticles in thermal performance of peristaltic flow of Eyring–Powell fluid model," *Journal of Thermal Analysis and Calorimetry*, vol. 143, pp. 1021–1035, 2021.

[38] T. Hayat, S. Qayyum, A. Alsaedi, and B. Ahmad, "Entropy generation minimization: Darcy-Forchheimer nanofluid flow due to curved stretching sheet with partial slip," *International Communications in Heat and Mass Transfer*, vol. 111, Article ID 104445, 2020.

[39] A. Riaz, R. Ellahi, S. M. Sait, and T. Muhammad, "Magnetized Jeffrey nanofluid with energy loss in between an annular part of two micro non-concentric pipes," *Energy Sources, Part A: Recovery, Utilization, and Environmental Effects*, pp. 1–20, 2020.

[40] A. Zeeshan, A. Majeed, M. J. Akram, and F. Alzahrani, "Numerical investigation of MHD radiative heat and mass transfer of nanofluid flow towards a vertical wavy surface with viscous dissipation and Joule heating effects using Keller-box method," *Mathematics and Computers in Simulation*, vol. 190, p. 1080, 2021.

[41] J. Buongiorno, "Convective Transport in Nanofluids," *Journal of heat transfer*, vol. 128, no. 3, pp. 240–250, 2006.

[42] M. W. Johnson and D. Segalman, "A model for viscoelastic fluid behavior which allows non-affine deformation," *Journal of Non-newtonian Fluid Mechanics*, vol. 2, no. 3, p. 255, 1977.

[43] Y. Wang, T. Hayat, and K. Hutter, "Peristaltic flow of a Johnson-Segalman fluid through a deformable tube," *Theoretical and Computational Fluid Dynamics*, vol. 21, no. 5, p. 369, 2007.

[44] A. Saleem, A. Qaiser, S. Nadeem, M. Ghalambaz, and A. Issakhov, "Physiological Flow of Non-Newtonian Fluid with Variable Density Inside a Ciliated Symmetric Channel Having Compliant Wall," *Arabian Journal for Science and Engineering*, vol. 46, no. 1, pp. 801–812, 2021.

[45] T. Hayat, M. Javed, and A. A. Hendi, "Peristaltic transport of viscous fluid in a curved channel with compliant walls," *International Journal of Heat and Mass Transfer*, vol. 54, no. 7-8, p. 1615, 2011.

[46] M. Kapoor, "Exact solution of coupled 1D non-linear Burgers' equation by using Homotopy Perturbation Method (HPM): A review," *Journal of Physics Communications*, vol. 4, no. 9, Article ID 095017, 2020.

[47] B. N. Kharrat and G. Toma, "Electronic Customer Relationship Management (E-CRM) and its Effect on Customer Retention of Selected E-Retail Companies in Lagos State, Nigeria," *Middle-East Journal of Scientific Research*, vol. 28, no. 2, p. 142, 2020.

[48] M. Qayyum and I. Oscar, "Least square homotopy perturbation method for ordinary differential equations," *Journal of Mathematics*, vol. 2021, Article ID 7059194, 16 pages, 2021.